Quantitative Radiation Thermometry Using Commercially Available High-Speed Video Cameras

Christopher B. Kostyk[*a] and Timothy K. Risch[a]
[a]NASA Armstrong Flight Research Center, PO Box 273, Edwards, CA, USA 93523-0273

ABSTRACT

In order to understand the risk posed to astronauts by electric arc-generated particles, high-speed, high-resolution, quantitative thermal imaging was needed. The measurement requirements appeared to be beyond the capabilities of commercial thermal imaging systems, but the particles were known to have a significant amount of emission in the visible spectrum. This challenge led to using commercially available, high-speed video cameras as imaging radiometers. Measured particle temperatures were consistent with predictions and other measurement data. The optical temperature measurement method, results, and conclusions are presented along with recommendations for further work.

Keywords: thermal imaging, high-speed video, radiometry, thermometry, pyrometry, quantitative

NOMENCLATURE

Acronyms

AFRC	Armstrong Flight Research Center
AFRL	Air Force Research Laboratory
FOV	field of view
ISS	International Space Station
NASA	National Aeronautics and Space Administration
ND	non-dimensional
NESC	NASA Engineering and Safety Center
Prefs	preferences
S/N	signal to noise
T_H	temperature, high
T_L	temperature, low

Symbols

A	area of a pixel, m^2
C_2	Planck's second constant, 14,388 μm-K
D	detector response function, A/W
$i_{b,\lambda}$	Planck distribution of total emissive intensity of a blackbody at temperature T, W/m^2-sr
I_0	signal (current) produced by the detector, A
T	temperature, K
ε_λ	spectral emissivity at wavelength λ
λ	wavelength, μm
Ω	effective solid angle of pixel, steridians

Subscripts

b	blackbody
b, λ	blackbody at wavelength λ
l	lower
u	upper

---

[*] chris.b.kostyk@nasa.gov; phone 661-276-5443; fax 661-276-2873; https://www.nasa.gov/centers/armstrong

1. MOTIVATION FOR THE WORK

Certain components on the International Space Station (ISS), particularly some fluid pumps under space environmental conditions, can have problematic restarts after power has been removed. The ISS team thus determined that the hot-swap of components on those circuits is preferable to removing power. Disconnecting components without removing power can, however, cause electrical arcing; the most severe condition considered was 82 A at 30 V over 0.055 s. Arcing can result in the generation of molten metal particles with enough thermal energy to damage extravehicular activity (EVA) Mobility Units (EMU) and put astronauts at risk. The ISS management requested that the National Aeronautics and Space Administration (NASA) Engineering and Safety Center (NESC) of the NASA Langley Research Center (LaRC) (Hampton, Virginia) perform an independent assessment of the risk to crewmembers due to the molten particles.[1] The associated measurement requirements appeared to be beyond the capabilities of commercial thermal imaging systems; however, the particles were known to have a significant amount of emission in the visible spectrum. Thus, the consideration of using commercially available, high-speed video cameras as imaging radiometers.

During initial project formulation activities, the NESC team identified members from Air Force Research Laboratory (AFRL) (Wright-Patterson Air Force Base, Dayton, Ohio) that had recently conducted a number of electrical arc tests in chambers simulating pressures from 20 to 740 torr. Initial testing at the AFRL facility, with representative voltage and current limits at pressures down to 0.1 torr, led to the conclusion that further testing in pressures representative of the ISS space environment (≈5×10-6 torr) was needed. During this time the NESC team determined that the molten metal particles needed to be measured along their trajectory with high-speed video cameras in a stereopsis configuration to determine particle count, size, speed, and temperature.

2. INITIAL SYSTEM REQUIREMENTS

Measurement system requirements were developed from two independent sources of information. The first source of information was a set of high-speed videos, showing low-pressure arcs (provided to the team by personnel from the Electrical Systems Branch of the Power and Control Division of the Aerospace Systems Directorate (AFRL/RQQE)). The second source of information was theoretical predictions of maximum potential particle temperatures, developed by a team member from the NASA Goddard Space Flight Center (GSFC) (Greenbelt, Maryland). Temporal resolution (exposure time and frame rate), spatial resolution, and spectral range requirements were generated from these sources.

2.1 Evaluation of Low-Pressure Arc High-Speed Videos

The AFRL personnel provided high-speed videos (2,000-fps, 5-μs exposure) taken from several of their low-pressure tests that showed bright particles being ejected from the arc location. The first video was taken from a test executed at 0.1 torr, and produced a particle that was estimated to be 0.67 mm (0.026 in) in diameter and ejected at 6.7 m/s (22 ft/s). A second video from a test executed at ambient conditions produced particles that were estimated to range in size from 0.3 to 1.0 mm (0.012 to 0.039 in) in diameter and ejected at speeds up to 9.1 m/s (30 ft/s). Both videos began with black images, with an arc event that saturated the entire detector for a frame, and then saturated the region around the discharge. The particles were also very bright, but it was not possible to know whether they were bright from their own luminance or simply reflecting the light from the discharge.

The NASA Armstrong Flight Research Center (AFRC) (Edwards, California) team members used those observations to assume that a new measurement system was needed that could accurately track a 1-mm (0.039-in) diameter particle with a minimum of 3 pixels of vertical and horizontal resolution. It was assumed that the particle could be ejected from the arc location in any direction at 6.7 m/s (22 ft/s) with a field of view (FOV) that extended 50 mm (2 in) on either side of the arc, with 1 pixel of blur. The resulting target spatial resolution was 0.33 mm/pixel (0.013 in/pixel), and temporal resolution was 20,000 fps (assuming the exposure time was the maximum allowed by the frame rate, 50 μs). The team had confidence that the exposure time could be reduced, therefore the blur could be reduced. The hope was to increase the resolution to 10 pixels across a 0.5-mm diameter particle (0.05 mm/pixel (0.002 in/pixel)); therefore, a camera detector/lens combination that would result in 300 to 2,000 pixels across a 10-cm (4-in) FOV was needed. Due to the uncertainty in particle ejection, an imaging detector would have to be used (streak cameras were not viable options).

2.2 Theoretical Predictions of Maximum Potential Particle Temperatures

The team used first principles to calculate the maximum potential particle temperatures given assumptions about the electrical energy, the estimated particle geometry, and the thermal properties. The result was a set of predictions for particles ranging in size from 2-3 mm (0.079-0.118 in) diameter. The maximum possible temperature for each of the three candidate materials (aluminum, copper, and stainless steel) could span a range from below the melting point up to the vaporization point of the metal (2743 K, 2835 K, and 3080 K, respectively) with varying levels of vapor generation. Thus it was understood that the particles could be significantly superheated, and emit a substantial amount of energy in the visible and infrared spectra.

3. MEASUREMENT OPTIONS EVALUATED

Initially, the team evaluated whether any commercially available infrared (IR) cameras could operate at 20,000 fps. Once the frame rate requirement was applied to available cameras, the spatial resolution and FOV criteria left no options. Cameras that could operate at thousands of frames per second required windowing down the pixel array so that either FOV or spatial resolution (or both) had to be compromised below useful levels.

The team then considered using conventional high-speed video cameras (that detect in the visible spectrum). While the team could obtain the spectral response function for a variety of high-speed video cameras, the team was not able to obtain enough information to calculate a predicted grayscale value for different particle temperatures and emissivities. The team thus needed to evaluate the feasibility of making the measurement during testing. No problem was posed, however, because the team needed a pair of visible high-speed video cameras to obtain the particle size, speed, and count data.

Two different pairs of commercially available high-speed video cameras were used for vacuum electric arc testing in two separate facilities. A pair of Photron FASTCAM SA-Z cameras (hereafter “Photrons”) (Photron, Tokyo, Japan) were used at one facility, and a pair of Vision Research Phantom v311 (hereafter “Phantoms”) (Vision Research, Inc., Wayne, New Jersey) were used at a second facility.

The Photrons could operate at 20,000 fps with a full pixel array (1024 by 1024 pixels); thus spatial resolution and FOV targets could be met. Previous experience with these cameras demonstrated that they did not have the problems of some other high-speed video cameras (for example: brightness fluctuation, image ghosting, duplicate, dropped, or out-of-order frames, et cetera). A 200-mm Nikon NIKKOR lens (Nikon USA, Melville, New York) was used with each camera to obtain the desired view. The exposure time was set to 5 μs; the resultant depth of field for this optical configuration (using a 91-cm (36-in) standoff distance and f32 aperture) was 27 mm (1.06 in).

The Phantoms were capable of windowing the pixel array down to 800 by 600 pixels and operating at 6,000 fps. This frame rate, and the resultant resolution and FOV, were sufficient for obtaining the desired measurement resolution targets. As with the Photrons, a 200-mm Nikon NIKKOR lens was used with each camera to obtain the desired view. The exposure time was set to 8 μs; the resultant depth of field for this optical configuration (using a 138-cm (54.5-in) standoff distance and f32 aperture) was 61.3 mm (2.41 in).

4. MEASUREMENT METHOD

The measurement method consisted of three parts: 1) performing a blackbody calibration of the camera/detector; 2) obtaining the characteristic 12-bit grayscale value for the particle from a high-speed video frame where no effect of participating vapor was present; and 3) converting that grayscale value to a temperature using the calibration curve and analytical tools. The first part, blackbody calibration, is discussed in section 4.1. The second and third parts (obtaining grayscale values and converting them to temperature), are discussed in section 4.2. Section 4.3 discusses various sources of error and uncertainty that were evaluated to better understand the measurement. Lastly, section 4.4 describes some measurement validation opportunities that occurred during the testing.

4.1 Calibration Method

The calibration method consisted of using a large blackbody (a Thermo Gauge Model 48-KW furnace) (Thermo Gauge Instruments, Inc., Fort Ashby, West Virginia) to generate a calibration curve for the detectors in the configuration used during testing. This method was applied to both the Photrons and the Phantoms.

To compensate for any transmission and reflective losses, the viewport windows from both vacuum chambers were obtained; the optical configuration was replicated for each camera while viewing the blackbody for calibration data collection (for example: identical standoff distances from both the blackbody and the arc site, applicable to both the viewport and the camera). Care was taken to pair the correct camera with the corresponding viewport. In each case, the camera was configured to have the same aperture setting and exposure time as was used during testing. A photograph of one of the vacuum chambers, as well as a photograph from the large blackbody calibration effort are provided as figure 1.

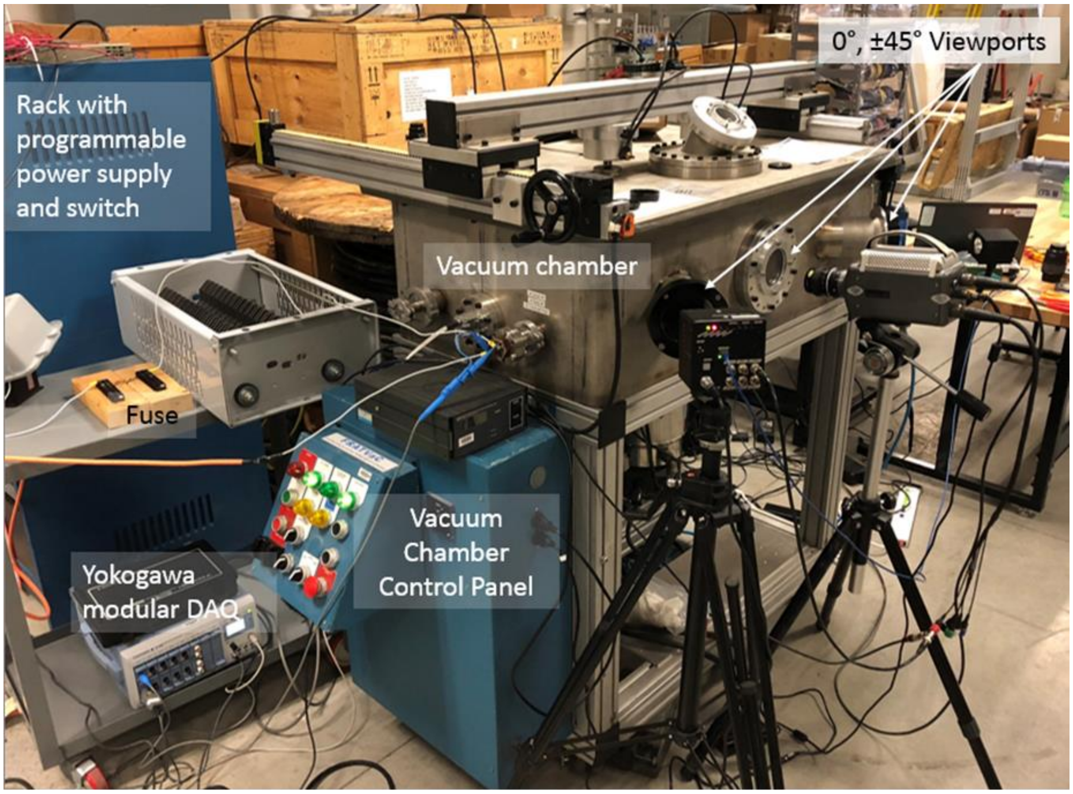

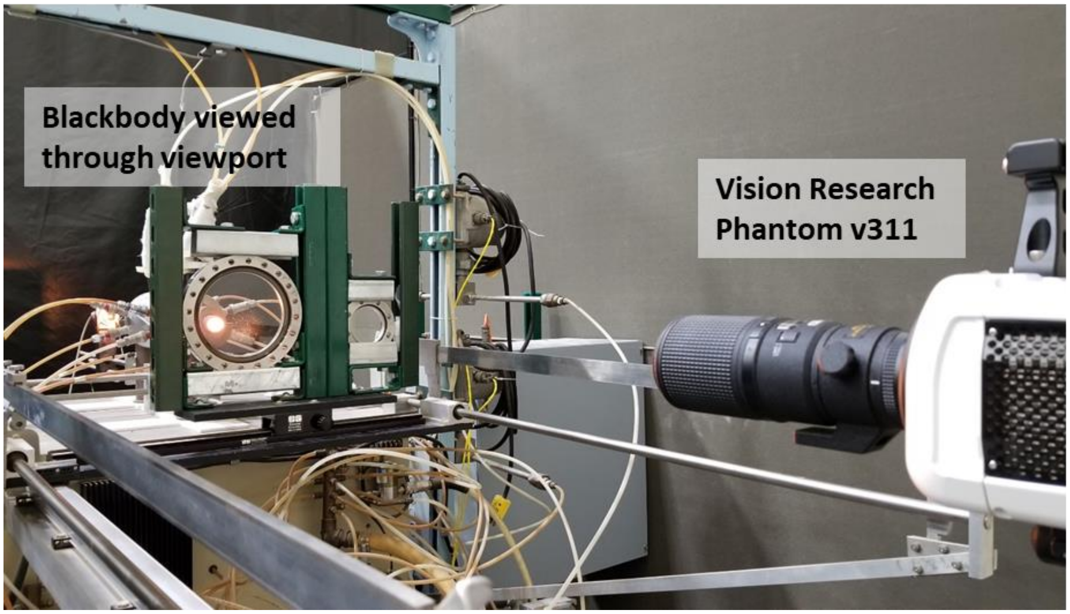

Figure 1. A photograph of one of the vacuum chamber test setups, top; and a photograph of one of the Vision Research Phantom v311 cameras (Vision Research, Inc., Wayne, New Jersey) being calibrated with the large blackbody, with the MSFC vacuum chamber viewports mounted for use during calibration to replicate the optical path for both cameras, bottom.

Prior to the blackbody operation, detector noise characterization images were taken (before and after two shading/taring operations, with and without the lens cap). A large area from the image of the blackbody aperture was used to obtain the 12-bit grayscale values, as shown in figure 2.

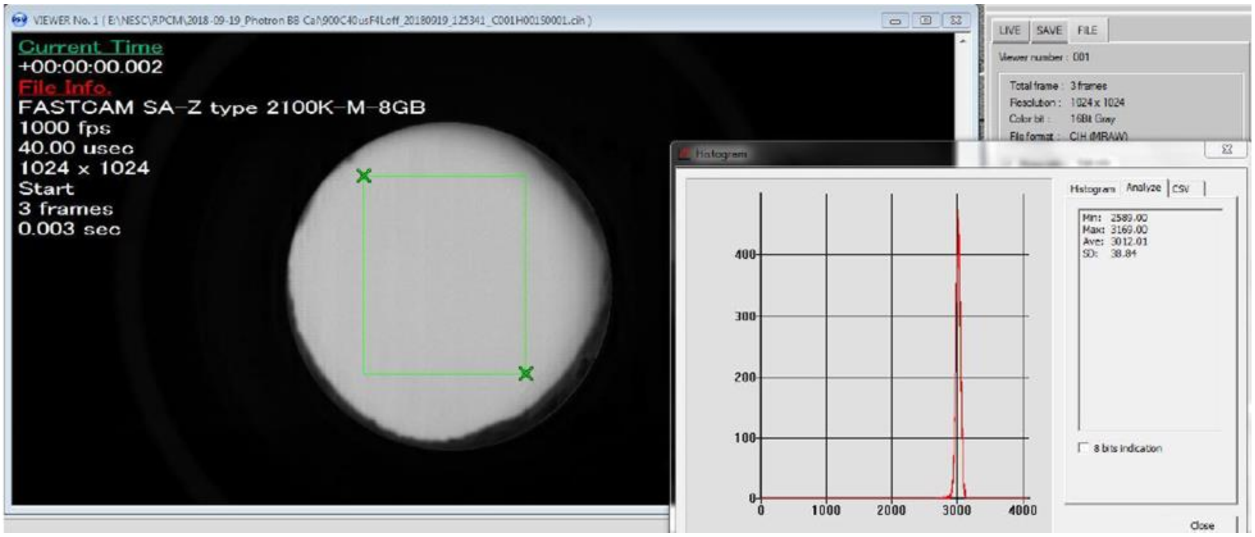
VIEWER No. 1 (E:\NESC\RPCM\2018-09-19_Photron BB Cal\900C40usF4Loff_20180919_125341_C001H00150001.cih)

Current Time
+00:00:00.002
File Info.
FASTCAM SA-Z type 2100K-M-8GB
1000 fps
40.00 usec
1024 x 1024
Start
3 frames
0.003 sec

Viewer number : 001
Total frame : 3 frames
Resolution : 1024 x 1024
Color bit : 16Bit Gray
File format : CIH (MRAW)

Min: 2589.00
Max: 3169.00
Ave: 3012.01
SD: 38.84

Figure 2. A screenshot from the Photron FASTCAM Viewer software (Photron, Tokyo, Japan), with region of interest reticle (green rectangle with "x" markers in top left and bottom right corners) showing the portion of the blackbody that was observed, along with the histogram that shows the tightness of the distribution of the grayscale values for that frame observing the blackbody at the specified temperature and using the prescribed optical configuration.

This data distribution was quite narrow, and the peak value was used to represent the grayscale value which resulted from the energy emitted at that temperature. For each temperature setpoint the signal generated by the blackbody was determined according to the relationship shown in equation (1):[2]

$$I_0 = A\Omega \int_{\lambda_l}^{\lambda_u} D(\lambda)\, i_{b,\lambda}(T,\lambda) d\lambda \tag{1}$$

where I_0 is the signal (current) produced by the detector (A), D is the detector response function (A/W), $i_{b,\lambda}$ is the Planck distribution of total emissive intensity of a blackbody at temperature T (W/m^2-sr), A is the area of a pixel (m^2), and Ω is the effective solid angle (steridians) of that pixel about the blackbody source. The requirement to quantify the A and Ω terms can be eliminated if the calibration is taken in the same optical configuration as the intended observation (standoff distance, optical path).

The MRAW format was used for the Photron videos, exporting 12-bit pixel values which were converted to usable histogram data directly in the Photron FASTCAM Viewer software (Photron, Tokyo, Japan). The CV2.5 software (Cine Viewer Application, Vision Research, Wayne, New Jersey) was used to export images for the Phantom video analysis from the Cine video format to Tagged Image File Format (TIFF) 12,36 format images for 12-bit pixel value analysis in the ImageJ Pixel Inspection Tool (hereafter "ImageJ") (United States National Institutes of Health open-source software).

For each temperature, the signal generated was calculated using equation (1), and the 12-bit grayscale was used to generate the calibration curve for the fully-replicated optical configuration. The temperature setpoints were chosen such that the intervals between them should result in approximately uniform spacing in terms of emitted energy and therefore grayscale (and therefore nonuniform temperature increments).

A final note on the calibration: as stated above, the temperature setpoints were nonuniform due to the selection of uniform radiative intensity increments. After the large blackbody calibration was performed with both the Photrons and the Phantoms, the calibration data were evaluated. The Phantoms exhibited an unexpected nonlinear response at the lower intensity levels, so additional lower-temperature calibration points were taken to ensure an accurate characterization of the curvature in the calibration curve. The additional lower-temperature data points were beneficial to the Phantoms, but yielded no benefit to the Photrons, which gave a very consistent response across the detector range from noise to saturation.

4.2 Temperature Determination

The process used to obtain temperature data along the particle trajectories using the high-speed video can be summarized as a seven-step process.

1) Perform pathfinder testing to determine the efficacy of the parameters required to obtain the data (f-stop, exposure time, frame rate, record length, and effect of potential noise sources such as ambient lighting, et cetera). Equipment and schedule permitting, perform a pre-test calibration.
2) Perform the actual testing and obtain the images of the particles to be used for temperature measurement. The optical configuration (viewports, cameras and positions, lenses, aperture settings, exposure time, et cetera) was frozen prior to testing; each set of optical parameters required its own calibration.
3) Perform post-test calibrations (in this case, post-test instead of pre-test due to project schedule). The calibration used the same equipment at the same standoff distances and settings as during testing.
4) Extract the grayscale values for the particles. Each particle image represents a collection of pixels that received radiated energy from portions of the surface in proportion to the cosine of the angle between the surface and the pixel. Therefore, the pixels that are imaging portions of the surface that are more normal will be brighter (assuming an isothermal surface). It is also known, however, that the particles may not be uniformly heated based on the flow of energy, and may not have a uniformly convex surface. For these reasons it was determined that the grayscale value to use was the peak grayscale and not the mean or mode. While it is not difficult to contrive scenarios in which this method might not be the appropriate method, the observations of the particles gave no indications of cavities, surface features, or grayscale distributions that would indicate that this approach was overly conservative for the subject application.
5) Use the grayscale value and the calibration curve to determine the approximate detector signal.
6) Choose an initial temperature to use in the confluence integral, as shown in equation (2):[2]

$$I_0 = A\Omega \int_{\lambda_l}^{\lambda_u} \varepsilon_\lambda \, D_i(\lambda) \, i_b(T,\lambda) \, d\lambda \tag{2}$$

   which differs from equation (1) and now includes the emissivity of the particles, ε_λ. The temperature is iterated until the signal produced is the same as that determined in step 5. The reported effort used macros and Microsoft Excel® Goal Seek (Microsoft Corporation, Redmond, Washington) to iterate and obtain the target temperature (a useful set of macros can be obtained from the NASA Armstrong Flight Research Center (AFRC) Technology Transfer Office).[2]
7) Finally, perform the optional step to repeat the fifth and sixth steps using a range of grayscale values to evaluate measurement uncertainty based on what the particular image of the particle looks like (grayscale distribution).

4.3 Sources of Error and Uncertainty

The uncertainties and errors associated with the measurement can be divided into two categories: measurand considerations (for example, the actual particle emission), and measurement system considerations.

Measurand considerations can be broken into three categories: spatial and temporal variations in temperature relative to the exposure time and image resolution, spectral emissivity uncertainty, and ambient/environment light sources and attenuation sources.

Measurement system considerations can be classified as being associated with detector noise, the sensitivity of the measurement system to uncertainty in emissivity, and detector repeatability.

4.3.1 Measurand Considerations

The considerations concerning the particles being measured were perhaps the most challenging at first simply because in this case knowledge about what is being measured is required in order to make the measurement. Furthermore, it is known that spectral emissivity is important and varies with temperature (the very quantity being sought); it was anticipated that there might not be much data in the temperature range of interest. These concerns were mitigated to such an extent as to render the measurement demonstrably feasible.

4.3.1.1 Spatial and Temporal Variations in Temperature Relative to Exposure Time and Image Resolution

The spatial variation of the grayscale values was consistently described as a single peak value with monotonically decreasing grayscale values away from the peak toward the edge of the particles. Occasionally there was a second peak region, but this is not surprising because the particles were superheated, very viscous fluid particles with often very dynamic surface topography. As stated previously, since the incident radiation is proportional to the cosine of the angle of the surface away from the focal plane, it is to be expected that the surface of the particle will appear brighter at the locations parallel to the focal plane, and decreasing toward the particle boundary. This alignment of expectation and reality gave confidence in the use of the peak grayscale value. An example is provided in figure 3.[3]

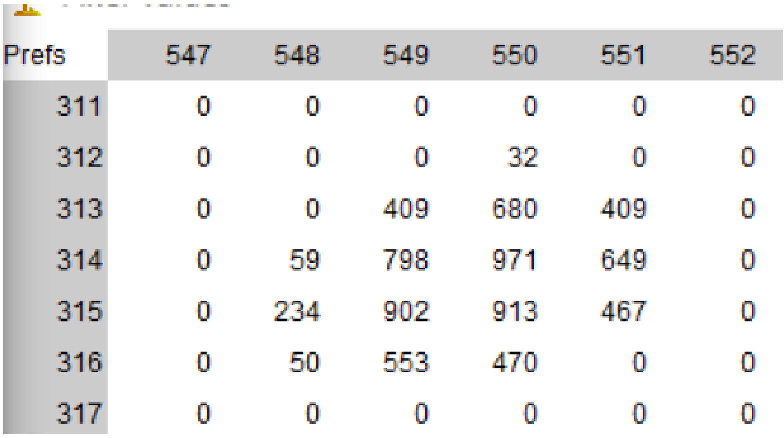

Prefs	547	548	549	550	551	552
311	0	0	0	0	0	0
312	0	0	0	32	0	0
313	0	0	409	680	409	0
314	0	59	798	971	649	0
315	0	234	902	913	467	0
316	0	50	553	470	0	0
317	0	0	0	0	0	0

Figure 3. The 12-bit grayscale values for a randomly-selected particle (TM5-03 particle #2, taken from Frame 12 and used for the temperature measurement). The screenshot from the ImageJ Pixel Inspection Tool (United States National Institutes of Health open-source software) used to interrogate the pixel values over and around the particle includes the horizontal and vertical pixel indices (gray shaded areas).

The temporal variation of the particle grayscale values was shown to occur on a time scale much longer than the exposure time, and commensurate with the radiative and evaporative cooling; therefore, this variation did not appear to pose a significant problem for the measurement.

4.3.1.2 Spectral Emissivity Uncertainty

Emissivity is an important parameter to know, because it relates how much radiant energy an object is going to emit relative to a blackbody (a pure, ideal emitter). Without knowledge of emissivity, thermal radiation cannot be properly analyzed. How much the uncertainty in the emissivity affects the measurement is measurement-system-dependent, and is discussed in section 4.3.2.1.

Finding the exact emissivity data that were needed proved challenging. Ideally, the team would utilize a reference document or data archive and find wavelength-dependent emissivity data for each material of interest (aluminum, copper, or stainless steel), at each temperature of interest. The spectral emissivity for liquid metals is not abundantly available, however, and less so for superheated liquid metals. Obtaining spectrally-resolved emissivity data for liquid metals involved a literature search and contacting numerous metal producers or suppliers. Some metals are more widely investigated than others. Several sources were found that reported spectral emissivity for liquid copper, one with data for liquid aluminum, and none reported data for liquid stainless steel. What was found is summarized below. Ultimately, what the team obtained proved to be sufficient.

Liquid Aluminum
Wavelength-dependent data for the index of refraction and extinction coefficient above the melting temperature of aluminum (950 K, 990 K, 1,030 K) were used to calculate the spectral emissivity profile, as shown in figure 4.[3] Since this reference was the only source of data available (that provided a spectral distribution and not just total hemispherical emissivity values), upper and lower bounding profiles were estimated at ±20 percent of the nominal profile.

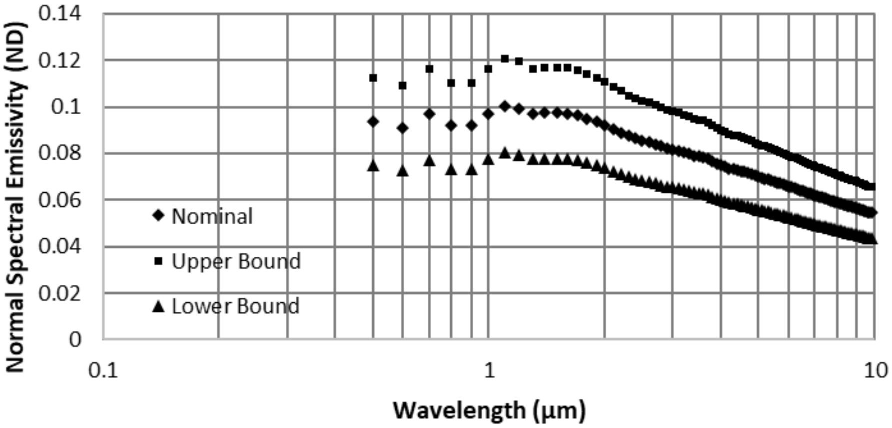

Figure 4. Normal spectral emissivity for aluminum calculated using ellipsometry data for the complex index of refraction found in the literature[3] with upper and lower uncertainty profiles determined using ±20 percent (consistent with uncertainty used for liquid copper based on the spread in literature, and uncertainty used for liquid stainless steel based on expert elicitation).

Liquid Copper

More data were found in the published literature for liquid copper, particularly from one research group. There were enough data that the team determined that the best approach would be to use the average spectral emissivity profile, and then use the high and low data points to generate bounding spectral emissivity profiles. The data, average, and bounding profiles are shown in figure 5 as found in the literature.[4-8]

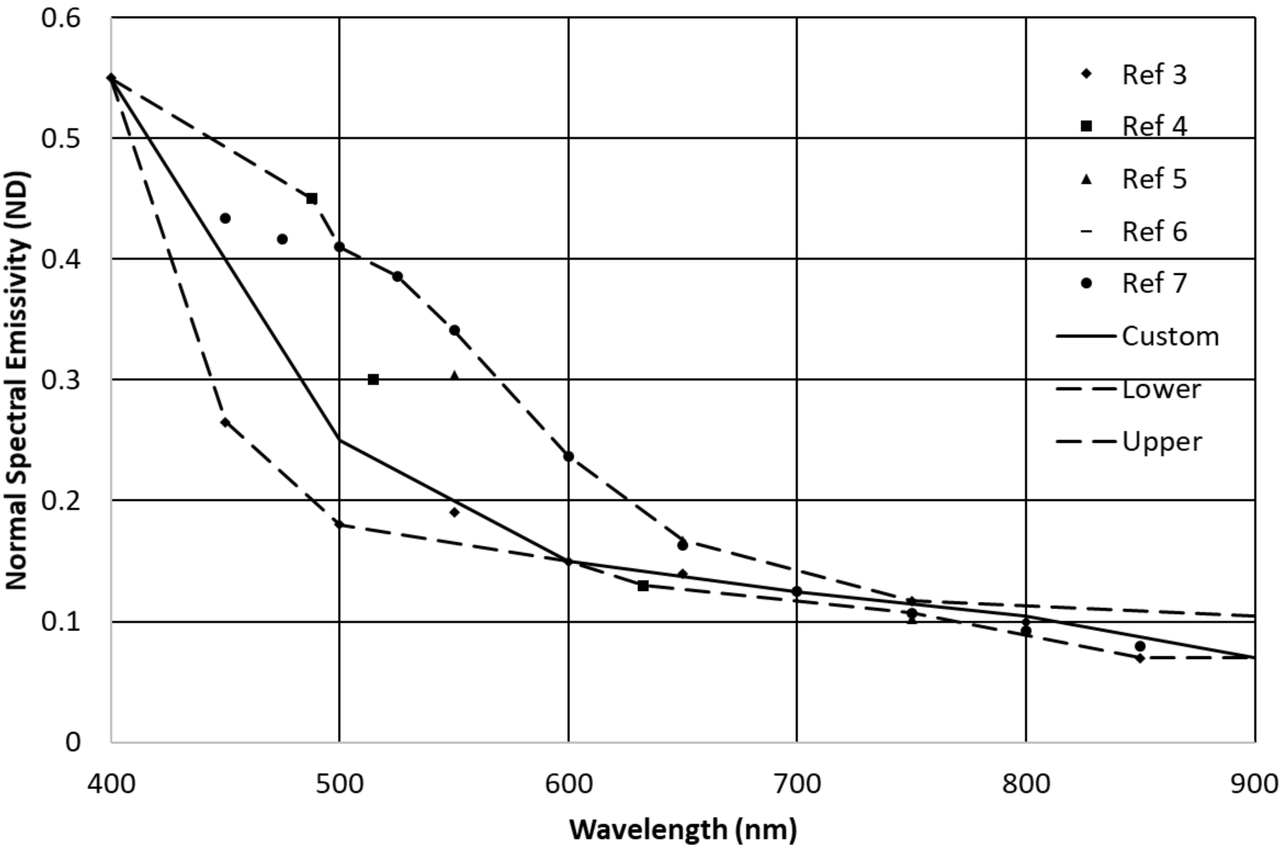

Figure 5. Normal spectral emissivity of liquid copper.4-8

Liquid Stainless Steel

A literature search for the spectral emissivity of liquid stainless steel yielded no results. Consultation with a number of specialty steel suppliers yielded no data for stainless steel; however, expert elicitation resulted in a reference[9] for the normal hemispherical emissivity of liquid iron and gave an opinion that it would likely be approximately 0.5, but as low as 0.4 and as high as 0.7. Another corroborating reference[10] was found. There being no data to justify any wavelength-dependence, a uniform value of 0.5 was used with lower and upper bounds of 0.4 and 0.7.

4.3.1.3 Ambient Environment Light Sources and Attenuation Sources

The light signal that is being measured has other potential sources of error: attenuation of the emitted signal from various media between the observed object and the detector, and augmentation from other sources of light that are incident on the detector.

4.3.1.3.1 Optical Signal Attenuation

The thermal emission (specifically, the visible to near-infrared spectrum, as relevant to the camera detector) travels from the object through the vacuum in the chamber, through a viewport, through air, to the camera lens (and air) to the camera detector. Attenuation through the atmosphere was negligible due to the use of visible wavelengths and the lack of any attenuating particles. Transmission loss through the optical system was rendered irrelevant because the optical path was replicated for each calibration (the cameras viewed the blackbody through the same viewports and at the same distances as during testing).

4.3.1.3.2 Ambient/Environment Light Sources

During the testing the thermal emission from the particles was not the only source of light. During the arc, event metal vapor was generated around the superheated liquid metal filament tip and ejected particles; the metal vapor was luminous due to participation in the electrical energy discharge. Immediately after the electrical energy discharge stopped ("discharge cessation") the metal vapor no longer emitted light, and the only source of light strong enough to generate a signal on the detector was the thermal emission of the particles and heated filament, as shown in figure 6.

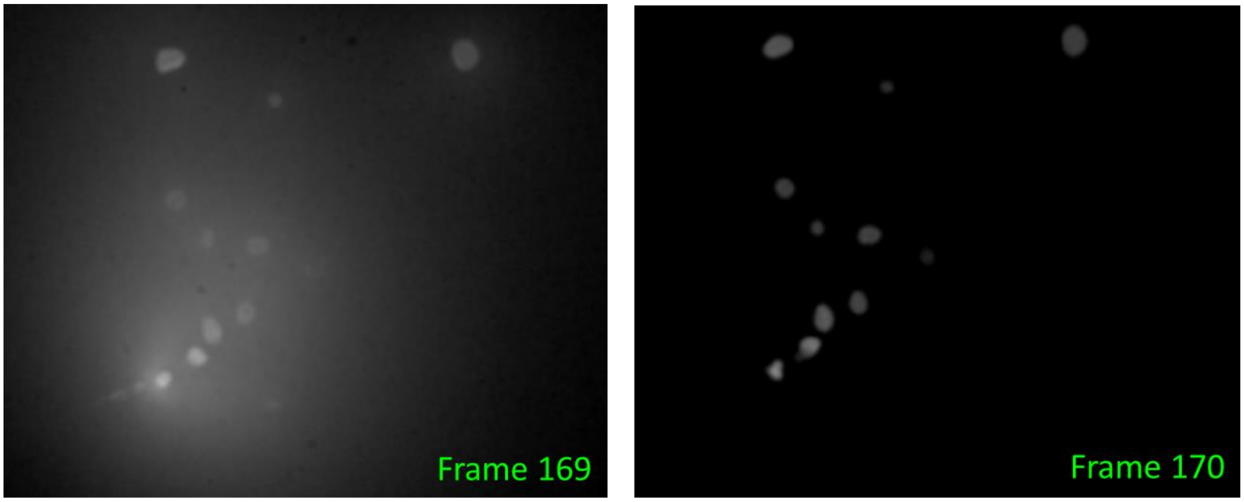

Figure 6. Sequential frames (test TM5-21) showing the luminous metal vapor surrounding the particles before discharge cessation (Frame 169, left), and non-emitting vapor surrounding the clearly visible, thermally emitting particles after discharge cessation (Frame 170, right). The frames were taken with a 8-μs exposure time and frame rate of 6,000 fps, so there was approximately 159 μs between the shutter closing on Frame 169 and opening on Frame 170.

When possible (that is, for the majority of measurements) measurements were made after the electrical arc event was complete, leaving ambient laboratory lighting as the only other light source. The noise generated by the ambient light in the laboratory (overhead lighting) could be characterized two ways: using the pre- and post-shading operation images (with and without the camera lens cap), as well as the quiescent frames from before and after the arc event. These evaluations were performed on both the Photrons and the Phantoms. The Photron ambient 12-bit grayscale noise level was

20 out of 4095, and the Phantom ambient 12-bit grayscale noise level was 60 out of 4095. An example of the results of this evaluation is provided in figures 7 and 8.

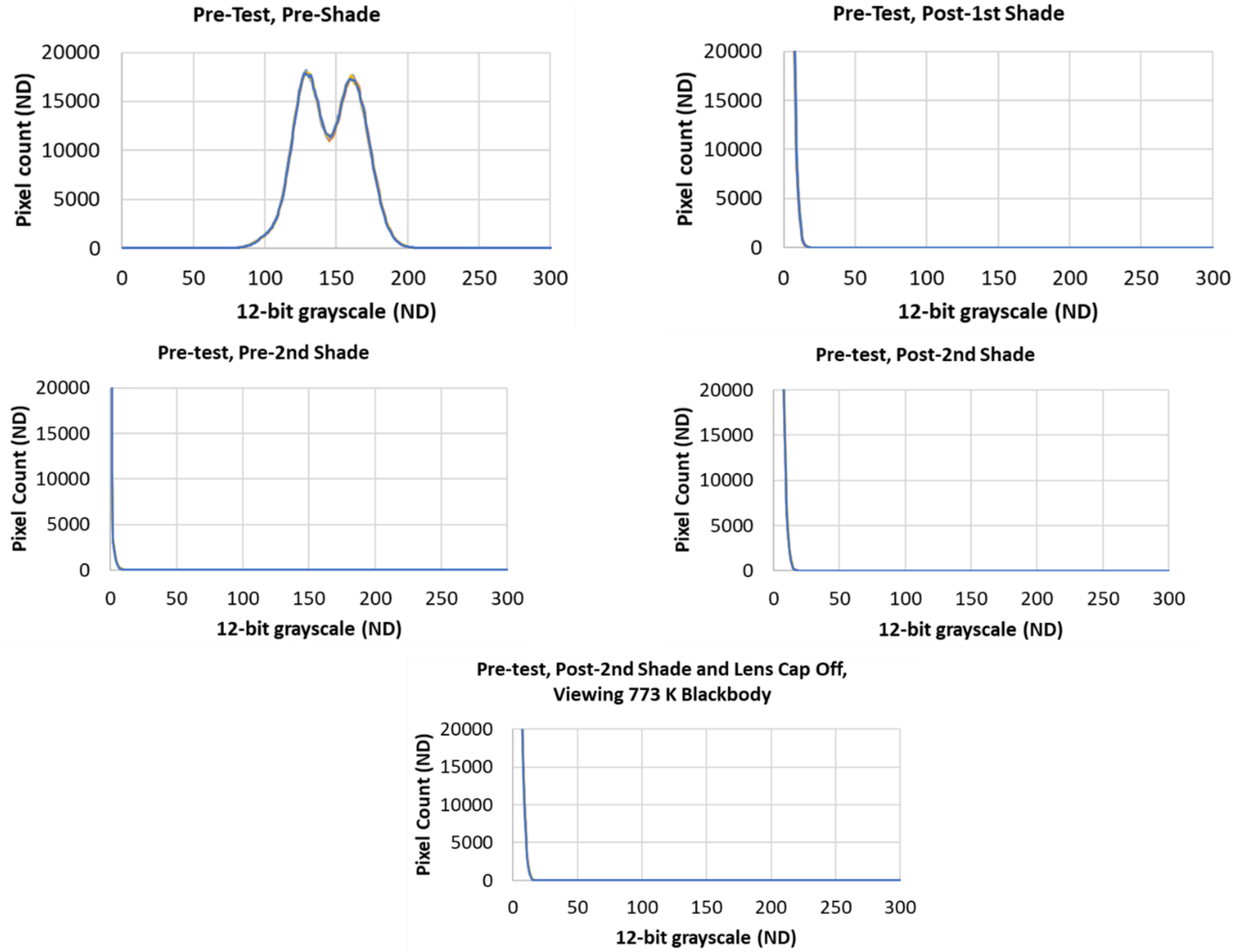
Pre-Test, Pre-Shade

Pre-Test, Post-1st Shade

Pre-test, Pre-2nd Shade

Pre-test, Post-2nd Shade

Pre-test, Post-2nd Shade and Lens Cap Off, Viewing 773 K Blackbody

Figure 7. Photron FASTCAM SA-Z camera (Photron, Tokyo, Japan) noise evaluation before and after shading operations.

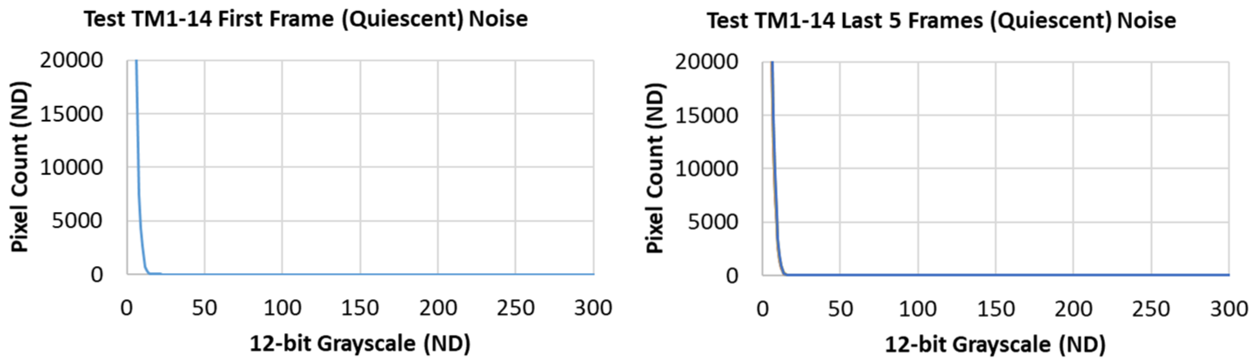
Test TM1-14 First Frame (Quiescent) Noise

Test TM1-14 Last 5 Frames (Quiescent) Noise

Figure 8. Photron FASTCAM SA-Z camera (Photron, Tokyo, Japan) noise evaluation using quiescent frames before and after a particular test.

The first three plots in figure 7 (top left and right, and middle left) show the detector noise level (lens cap on) when the camera was first turned on, after the first shading operation, and then before the second shading operation (approximately

20 min later). The next two plots (middle right, and bottom) show the noise level after the second shading operation, and after the lens cap is removed and the camera is observing the blackbody at 773 K in ambient lighting. The noise level – ever since the first shading operation at the very beginning of the calibration run – was monotonically decreasing in pixel count for 12-bit grayscale values of 0 to 20. This noise profile remained stable throughout the use of the camera.

Figure 8 shows the noise level evaluated using the quiescent frames before and after the test. The noise profile was the same as shown in figure 7, whereas the data shown in figure 7 were taken six months later, during the post-test calibrations using the same optical configuration (standoff distance, f-stop, exposure, and viewport). The noise levels thus evaluated resulted in significant signal-to-noise (S/N) values for the particles observed (using the 12-bit grayscale values as the "signal" and "noise" levels). The Photrons observed 31 particles with 12-bit grayscale S/N range of 5 to 164 and an average value of 36. The Phantoms observed 212 particles with S/N range of 0.5 to 52, with an average value of 13. There were 13 particles with S/N < 2.0, so the majority of the observed particles (94 percent) were measured with S/N greater than 2.0. While the Phantoms carried a measured noise level of 60 counts, the majority of the pixels were zero; a very small percentage of the pixels was nonzero. An example is provided in figure 9.

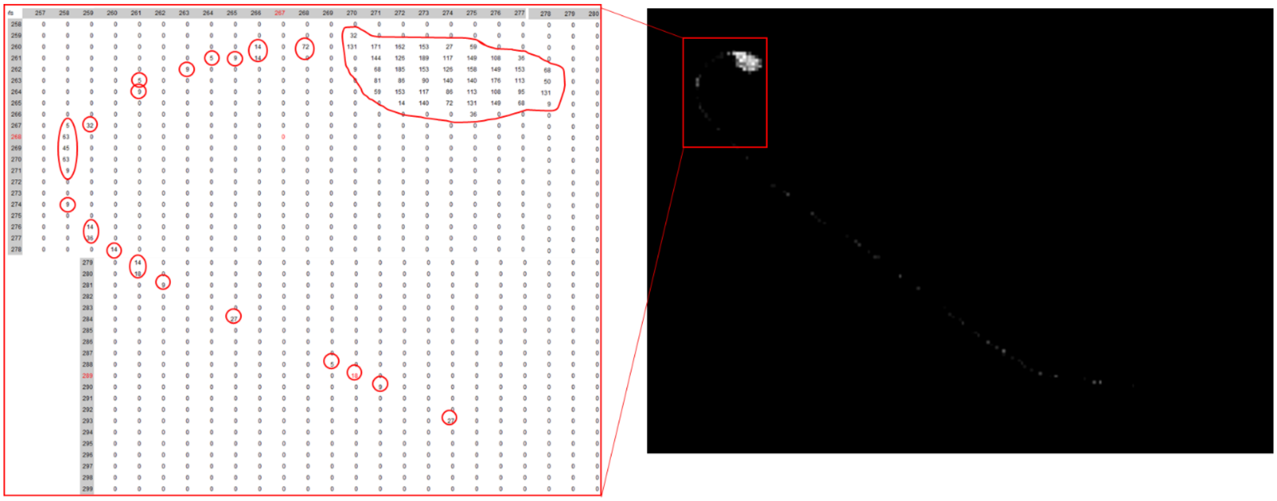

Figure 9. The dim image of the partially-molten filament fragment, right, observed with one of the Vision Research Phantom v311 cameras (Vision Research, Wayne, New Jersey), and the 12-bit grayscale values of the pixels shown by several ImageJ Pixel Inspection Tool (United States National Institutes of Health open-source software) windows stitched together. The screenshots from ImageJ shown on the left are subsets of the right-hand image from the video, the immediate vicinity of the superheated molten head of the filament. The nonzero grayscale values of the partially-molten filament fragment are circled in red, while the rest of the pixels are at zero. This condition of nonzero grayscale values over the particles, and zeros across the rest of the image, was extremely common during video analysis.

4.3.2 Measurement System Considerations

In addition to sources of error or uncertainty related to what is being measured, there are also sources of error or uncertainty related to the system being used to make radiometric temperature measurements. Considerations pertinent to the measurement system are system sensitivity to emissivity uncertainty, and detector short-term and long-term stability.

4.3.2.1 System Sensitivity to Emissivity Uncertainty

The system sensitivity to surface emissivity uncertainty will either attenuate or magnify into an uncertainty in temperature measurement based on the wavelength of the light being used by the measurement system. This sensitivity was evaluated using two different methods.

The first method used to evaluate the radiometric temperature measurement system sensitivity to emissivity uncertainty was to assume a monochromatic detector. The closed-form analytical solution (given Wien's approximation) is as shown in equation (3):[2]

$$\frac{d\ln T}{d\ln \varepsilon_\lambda} = -\frac{\lambda T}{C_2} \tag{3}$$

where C_2 is Plank's second constant and equal to 14,388 μm-K. The wavelength dependency in the derivative means that a longer wavelength detector will be more sensitive to uncertainties in emissivity and amplify those uncertainties into an uncertainty in the temperature measurement. Assuming the Photron camera is used to measure a 2300-K aluminum particle (figure 6 for spectral emissivity) at 700 nm, the spectral emissivity could be stated as 0.1 ±0.02. The resulting temperature uncertainty would be 51 K (2.2 percent). The resulting temperature uncertainty for a mid-wave infrared camera (assuming a 4-μm wavelength and corresponding spectral emissivity) would be closer to 17 percent.

The Photron camera is not a narrow-band system, so a numerical method can be used to evaluate the performance of the system. If the ±20-percent spectral emissivity profiles for aluminum are used to calculate a corresponding temperature uncertainty range, the result is a ±2-percent temperature variation from the results of using the nominal spectral emissivity curve in the calculation (notably close to the results using the simplified approach assuming a monochromatic detector). The results of the closed-form analytical and numerical investigations into the system sensitivity to emissivity uncertainty provided the team with important confidence in the results.

4.3.2.2 Detector Stability

The team evaluated the stability of the detector response in the short term (several frames in a sequence) as well as in long-term stability (exposed to the same stimulus over days, weeks, months).

Short-term stability was evaluated many times, by comparing grayscale distributions for groups of sequential frames. Figure 10 shows an example of using the Photron Fastcam Viewer software to obtain the grayscale distributions for several sequential frames and compare them (see figure 11). The comparison in figure 11 is typical of what was observed for both the Photrons and the Phantoms: very consistent image stability from one frame to the next when exposed to the same stimulus.

The long-term stability of the detector response was (partially) addressed in the discussion surrounding the noise stability from testing to calibration six months later. To truly evaluate the stability of the detector over the long term the response of the detector to similar stimuli must be evaluated. This evaluation can be accomplished by considering the calibration results for the cameras.

The calibration data were obtained over several months. One particular camera will be shown as an example of what was observed. Figure 12 presents three different calibration datasets with distinct marker styles to show that the three different datasets are highly correlated and indistinguishable.

To further illustrate the stability, two different temperatures from the calibration data above are compared: a lower temperature (1373 K) and a higher temperature (2079 K). The grayscale values are shown in the subplots of figure 12. The method used to evaluate the detector stability using the calibration data is illustrated in figure 13.

For the 2079-K data, the bounding peak grayscale values of 3483 and 3815 equate to blackbody temperatures of 2045 K and 2085 K (-1.6-percent and 0.3-percent errors in temperature, respectively). The calibration curve appears to produce values just above and below the target temperature using these bounding grayscale values. This spread was the widest in the calibration data for that camera.

This long-term stability as demonstrated by taking the spread in calibration data (taken over months) and converting to spread in resulting temperature measurements was considered more than satisfactory for the purposes of the assessment. In this case, "long-term" is defined as a time scale exceeding the amount of time the systems were used. The Photrons and Phantoms were each used for approximately one month of testing.

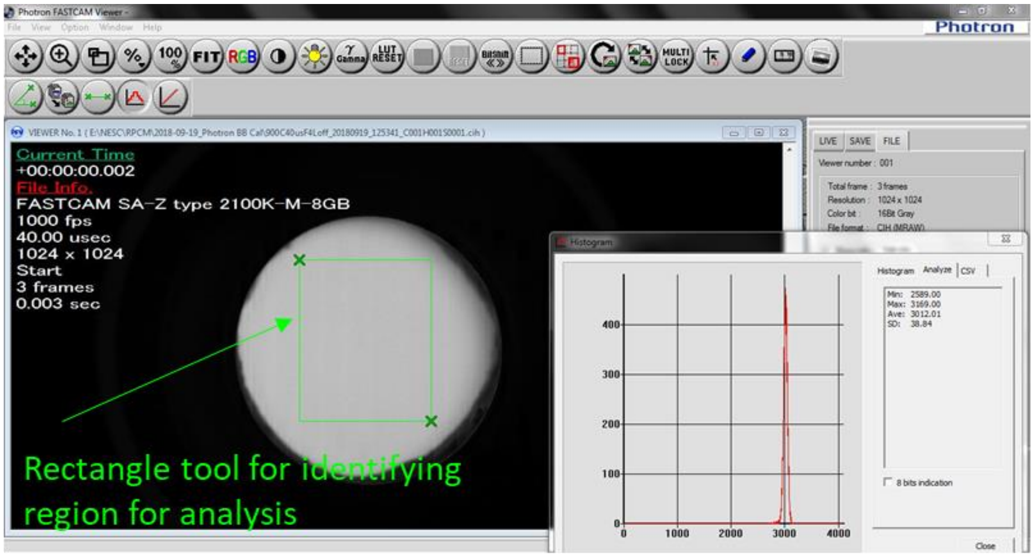

VIEWER No. 1 (E:\NESC\RPCM\2018-09-19_Photron BB Cal\900C40usF4Loff_20180919_125341_C001H001S0001.cih)

Current Time
+00:00:00.002
File Info.
FASTCAM SA-Z type 2100K-M-8GB
1000 fps
40.00 usec
1024 x 1024
Start
3 frames
0.003 sec

Rectangle tool for identifying region for analysis

LIVE SAVE FILE

Viewer number : 001

Total frame : 3 frames
Resolution : 1024 x 1024
Color bit : 16Bit Gray
File format : CIH (MRAW)

Histogram Analyze CSV

Min: 2589.00
Max: 3169.00
Ave: 3012.01
SD: 38.84

☐ 8 bits indication

Figure 10. Screenshot of the area used for analyzing the stability of the detector response to the blackbody over several frames.

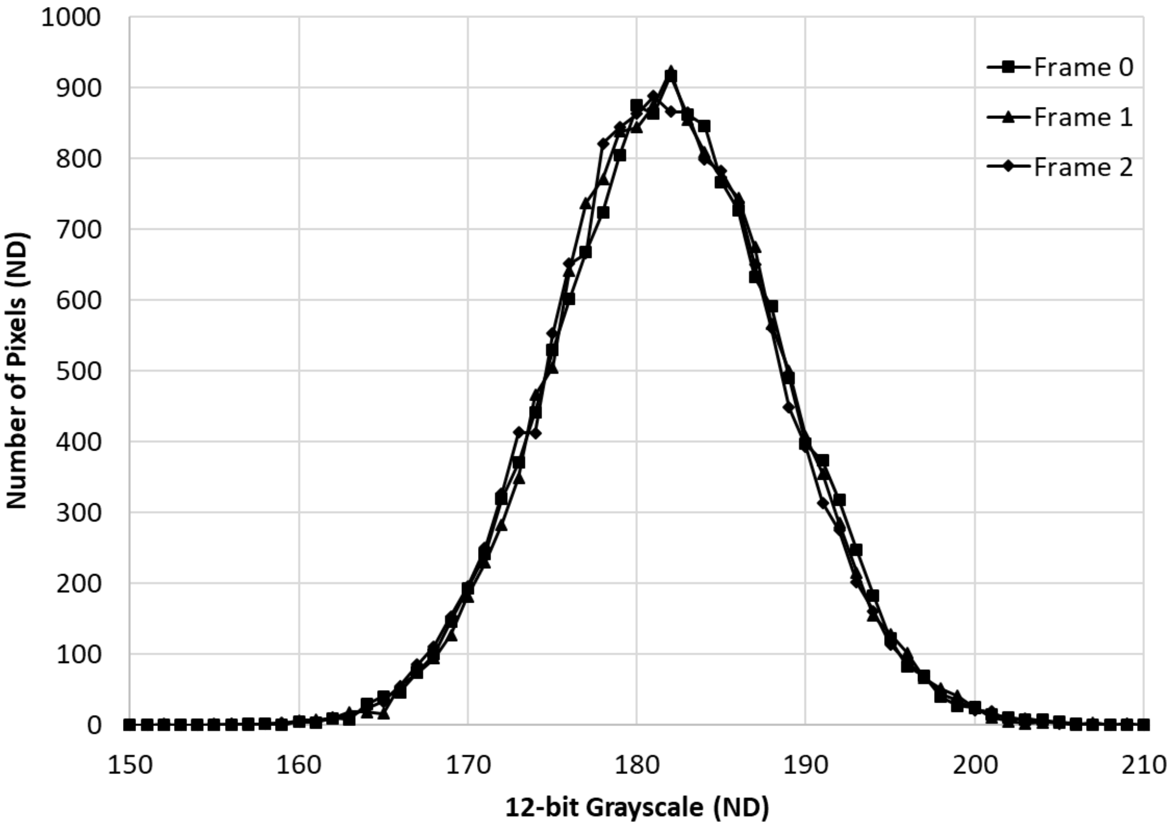

Figure 11. Grayscale value distribution for three frames in a row from the Photron FASTCAM SA-Z camera (Tokyo, Japan), typical of what was observed.

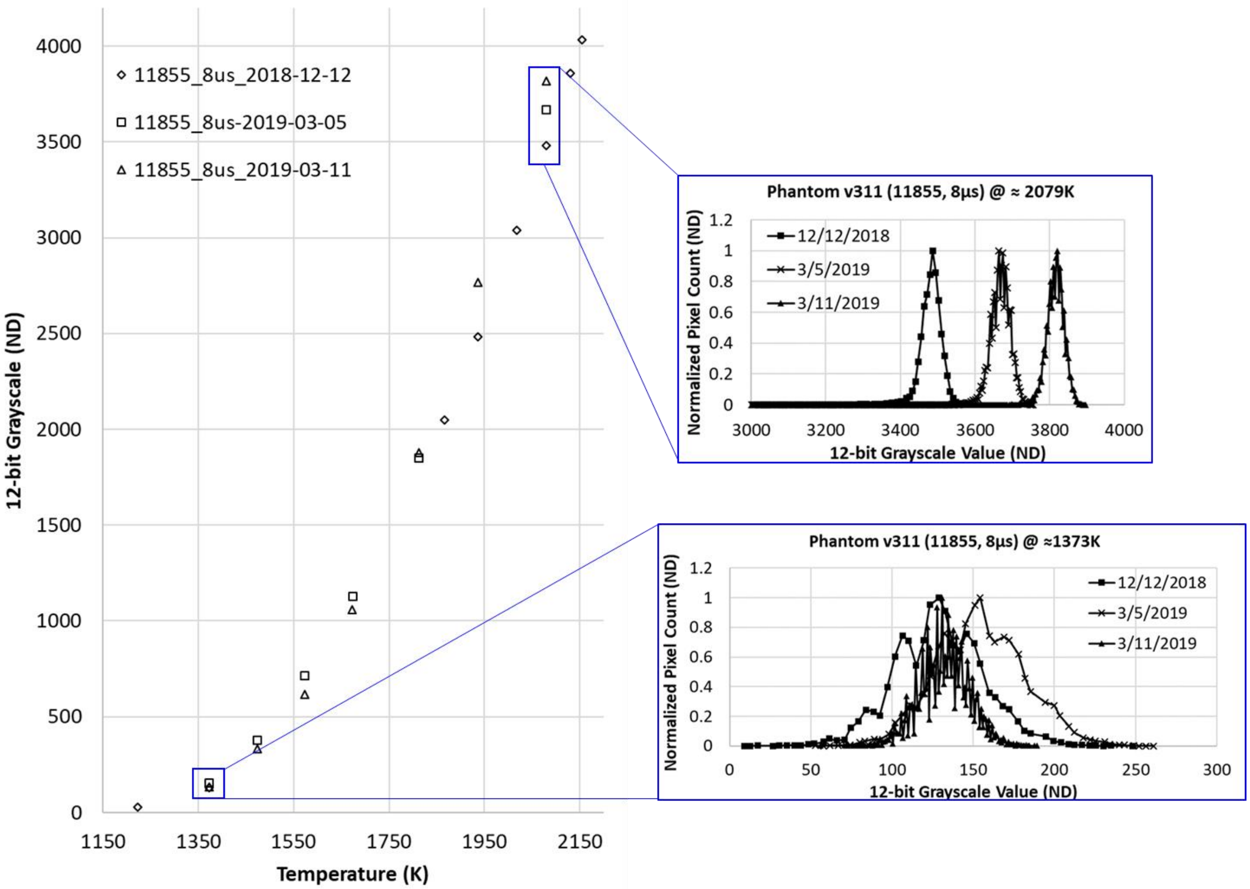

Figure 12. Vision Research Phantom v311 camera (Vision Research, Wayne, New Jersey) calibration sets distinguished by different markers; the calibration data points having the least and greatest separation are shown in subplots.

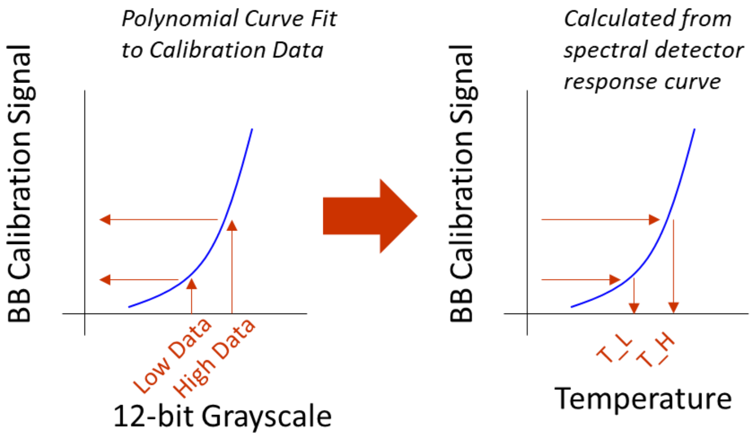

Figure 13. Diagram of the method used to evaluate the calibration sensitivity to low and high data from the calibration runs by the corresponding low and high bounding temperature estimates that would result.For the 1373-K data, the bounding peak grayscale values of 128 and 154 equate to blackbody temperatures of 1426 K and 1431K (3.85-percent and 4.22-percent error in temperature, respectively). The calibration curve appears to overpredict these lower temperatures by less than 5 percent using these bounding values.

4.4 Validation Opportunities

Fortunately, despite the problems that could affect the measurement, there were some inherent validation opportunities present in the test datasets. Typical arc events resulted in the filament tip being propelled from the arc site (figure 14A) and ejecting particles in every direction (figure 14B). There were several instances, however, of filaments fusing to the cathode plate (negative terminal) and then Joule heating (resistively heating) until they melted (figure 14C). The temperature of the filaments in these cases were known to be within a band around the melting temperature (or melting temperature range, in the case of an alloy), meaning that, if the system were accurate ("system" is defined here as the combination of the camera system and data reduction method), the grayscale values of the luminous filaments should result in a temperature value near this intrinsic material property.

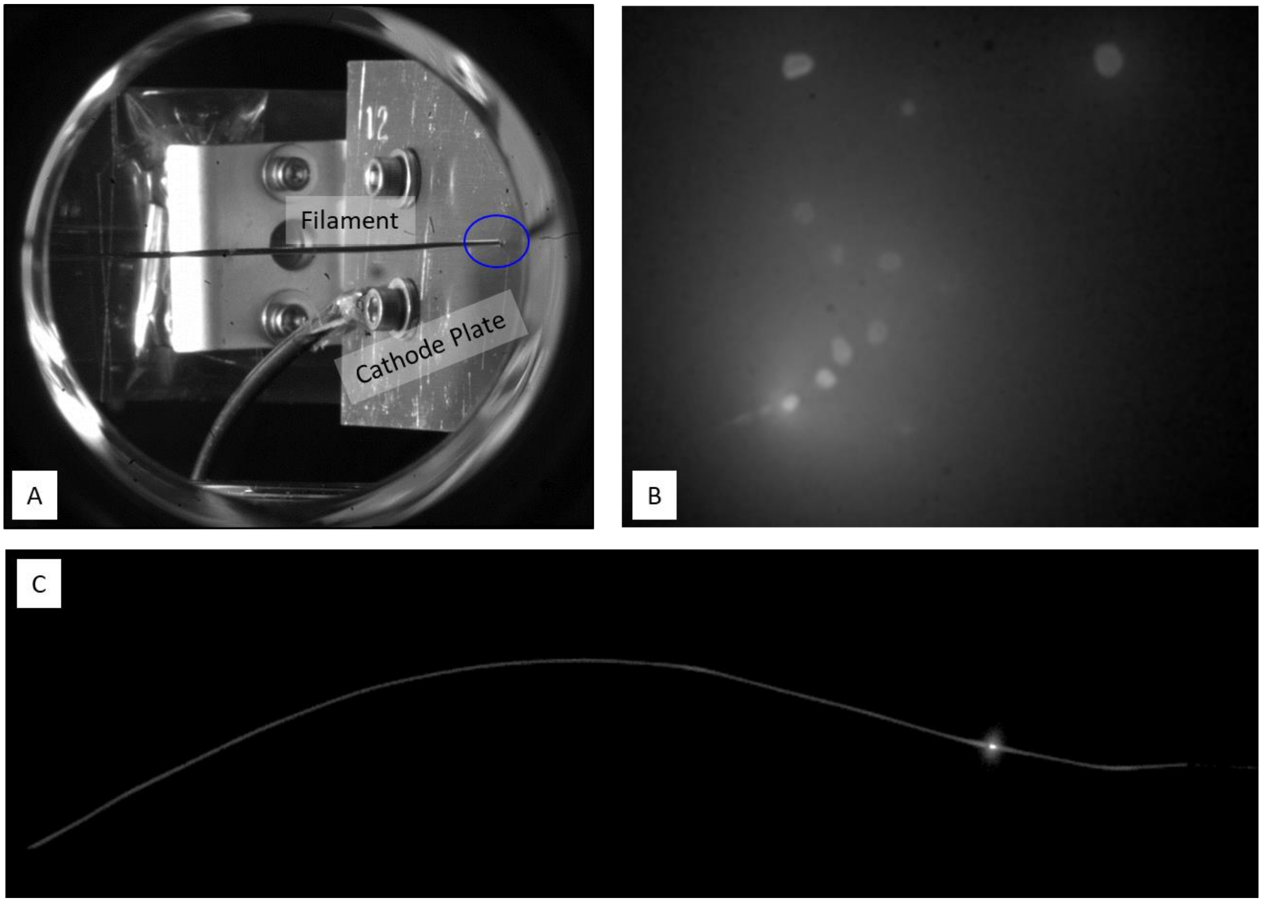

Figure 14. An image of the arc location, with anode (positive) filament going from left to right across the center of the viewport and coming into contact with the cathode (negative) plate on the right of the image, [A]; typical ("archetypal") particle generation where the filament is propelled from right to left away from the arc site, ejecting super-heated particles that are surrounded by a metal vapor cloud that is luminous due to participation in the electrical energy flow until discharge cessation, [B]; and one example of a test wherein the tip of the filament fused to the cathode plate, resulting in Joule heating (resistive heating) the filament until it softened, melted, and fell apart, [C].

These cases were valuable for validating the method and equipment used; furthermore, these validation cases could be used both quantitatively and qualitatively. Quantitatively, the measurement (including pixel grayscale distribution) could be compared against the approximately known temperature. Qualitatively, the grayscale could be compared to the grayscale values of the particles from the normal discharge events; if the grayscale values of particles produced from a normal discharge were far brighter, then it would be understood that the particles were far hotter than the melting temperature.

The Photron cameras observed one test during which the filament melted and fell apart and the electrical discharge stopped almost immediately. The electric arc discharge saturated the camera and produced stray light that interfered with the particle emission, therefore valid measurements could only be made after cessation of the discharge. The filament was made from 304 stainless steel, which has a melting range of 1673-1723 K. The temperature was measured as 1743 K. This incident was considered a successful validation of the system.

During later testing, the Phantoms also observed several filaments that melted and broke apart. For the Phantoms, the temperature range of 1650-1750 K spans 12-bit grayscale values of 506-847. Several tests did not have discharge cessation to allow valid measurements, but several tests did, and the gray scale values along the apparently molten filament fragment spanned the grayscale range corresponding to the melting temperature range, thus validating the same approach using the Phantoms.

5. MEASUREMENT SYSTEM CHARACTERIZATION RESULTS

The high-speed video cameras operating in the visible spectrum used during the assessment were proven to provide radiometric temperature measurements that satisfied project requirements. Table 1 summarizes the temperature ranges for the various metals for each camera system as used.

Table 1. Material-specific temperature measurement limits, K, for the high-speed cameras used during the assessment.

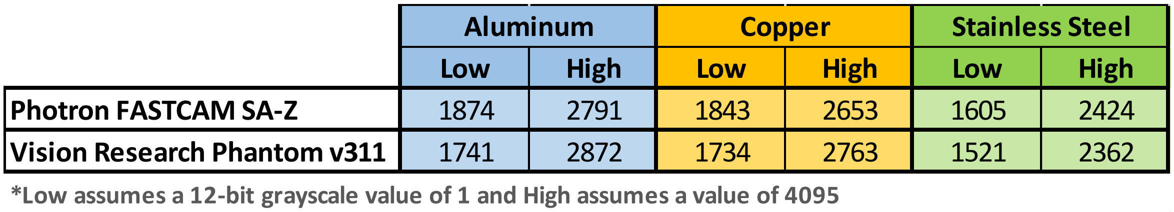

	Aluminum		Copper		Stainless Steel	
	Low	High	Low	High	Low	High
Photron FASTCAM SA-Z	1874	2791	1843	2653	1605	2424
Vision Research Phantom v311	1741	2872	1734	2763	1521	2362

***Low assumes a 12-bit grayscale value of 1 and High assumes a value of 4095**

It should be noted that these temperature limits are given for the as-implemented configuration. There is some ability to tailor the temperature range to different applications by modifying parameters such as exposure time, f-stop, and standoff distance. Both the Photron camera and the Phantom camera were used with the aperture set at f32. The Photron was used with a 5-μs exposure time; the Phantom temperature limits are shown for the case in which the 8-μs exposure time was used. The limits of the camera systems (minimum or maximum exposure times, minimum or maximum aperture setting, and minimum or maximum standoff distances) were not explored during the effort.

6. CONCLUSIONS

Commercially available high-speed video cameras operating in the visible spectrum can be used for quantitative thermal imaging of aluminum, copper, and stainless steel objects between 1500-2900 K with high spatial and temporal resolution. The investigations into errors and uncertainties demonstrated sufficient accuracy for the subject application, and were corroborated by unplanned validation opportunities that occurred during testing.

7. RECOMMENDATIONS FOR FURTHER WORK

The systems used during the reported effort could be further evaluated for blackbody temperature measurement limits to understand the full range of applicability of those systems. That effort seems particularly desirable because most applications of quantitative thermal imaging involve temperatures lower than those of superheated molten metal. Additionally, the National Aeronautics and Space Administration (NASA) owns a variety of high-speed video cameras. Some cameras have technical problems (for example, ghosting) that would necessarily remove them from consideration, but other cameras could easily be evaluated for similar use. The potential use of high-speed infrared cameras would be helpful.

REFERENCES

[1] West, T. (S.) and Hernandez-Pellerano, A., [International Space Station (ISS) Remote Power Controller Module (RPCM) Hot Mate/Demate During Extravehicular Activity (EVA)], NASA/TM-2019-220421/Volumes 1 & 2 (2019) (distribution limited to U.S. persons only).

[2] Risch, T. K., [User's Manual: Routines for Radiative Heat Transfer and Thermometry], NASA/TM-2016-219103 (2016).

[3] Havstad, M. A., McLean II, W., Self, S. A., “Apparatus for the measurement of the optical constant and thermal radiative properties of pure liquid metals from 0.4 to 10 μm,” Rev. Sci. Instrum. 64(7), 1971-1978 (1993).

[4] Nagata, K., Nagane, T. and Susa, M., “Measurement of normal spectral emissivity of liquid copper,” ISIJ International, 37(4) 399-403 (1997).

[5] Krishnan, S. and Nordine, P., “Optical properties and emissivities of liquid metals and alloys,” in NASA Lewis Research Center, Workshop on the Thermophysical Properties of Molten Materials, 143-160 (1993).

[6] Watanabe, H., Susa, M. and Nagata, K., “Discontinuity in normal spectral emissivity of solid and liquid copper at the melting point,” Metallurgical and Materials Transactions A 28A, 2507-2513 (1997).

[7] Watanabe, H., Susa, M., Fukuyama, H. and Nagata, K., “Near-infrared spectral emissivity of Cu, Ag, and Au in the liquid and solid states at their melting points,” International Journal of Thermophysics 24(4), 1105-1120 (2003).

[8] Watanabe, H., Susa, M., Fukuyama, H. and Nagata, K., “Phase dependence (liquid/solid) of normal spectral emissivities of noble metals at melting points,” International Journal of Thermophysics 24(1), 223-237 (2003).

[9] Dastur, M..N. and Gokcen. N. A., “Optical temperature scale and emissivity of liquid iron,” Metals Transactions 185, 665-667 (1949).

[10] Kobatake, H., Khosroabadi, H. and Fukuyama. H., “Normal spectral emissivity measurement of liquid iron and nickel using electromagnetic levitation in direct current magnetic field,” Metallurgical and Materials Transactions A (43A) 2466-2472 (2012).